Bond breaking and bond making in tetraoxygen: analysis of the O2(X3Sigma(g)-) + O2(X3Sigma(g)-) O4 reaction using the electron pair localization function.

Michel Caffarel, Anthony Scemama, Alejandro Ramírez-Solís

*) Corresponding author: alex@buzon.uaem.mx

Bond breaking and bond making in tetraoxygen: Analysis of the $O_2(X^3\Sigma_g^-)+O_2(X^3\Sigma_g^-) \leftrightarrows O_4$ reaction using the Electron Pair Localization Function.

Michel Caffarel[a)], Anthony Scemama[a)], and Alejandro Ramírez-Solís [b)*]

[a)] *Laboratoire de Chimie et Physique Quantiques, CNRS-IRSAMC Université de Toulouse, France.*

[b*)] *Depto. de Física, Facultad de Ciencias, Universidad Autónoma del Estado de Morelos. Cuernavaca, Morelos 62209. México.*

(Dated: September 16, 2008)

Tetraoxygen, O_4, is a molecule of great importance playing a central role in a variety of chemical and physical processes. Among them we can cite the dynamics of the atmospheric processes involving ozone, the understanding of the anomalous magnetism of liquid oxygen, the possible explanation of the structural and optical properties of the ϵ solid phase of oxygen, and also the possible use of polyoxygen species as high energy-density (HED) materials. The reaction leading to the formation of tetraoxygen (with total spin S=0) from the interaction of two two-open shell (S=1) oxygen molecules requires complex electronic spin-space recouplings that can only be properly described with multiconfigurational methods. The understanding of the simultaneous intramolecular bond-breaking and the intermolecular bond-making processes that occur during this reaction is very difficult to achieve by analyzing the wavefunction composition along the reaction coordinate or by following the evolution of the total or orbital electronic density since the active orbitals are delocalized over the four nuclei. In order to achieve this goal, we study the nature of the electron pairing at the two most important critical points of the singlet potential energy surface (PES) of the $2O_2 \leftrightarrows O_4$ reaction and, also, its evolution along the reaction coordinate using the Electron Pair Localization Function (EPLF) [A. Scemama, P. Chaquin and M. Caffarel, J. Chem. Phys. **121**, 1725 (2004)]. To do that, the 3D-topology of the EPLF calculated with quantum Monte Carlo (at both variational and fixed-node-diffusion Monte Carlo levels) using Hartree-Fock, multiconfigurational CASSCF, and explicitly correlated trial wave functions is analyzed. At the O_4 equilibrium geometry the EPLF analysis reveals four equivalent covalent bonds and a couple of lone pairs on each oxygen atom. At the singlet transition state the EPLF reveals a very intricate electronic structure where the O_2 molecules (in C_2 symmetry) transform two π bonds each into lone pairs and, simultaneously, a couple of new intermolecular σ bonds are being created by the coupling of two same-spin electrons provided by

each O_2 moiety. Finally, the EPLF allows to visualize the sequence of topological transformations of the electron pairings along the reaction coordinate from the transition state to the dissociated fragments. As a general conclusion, we emphasize the usefulness of the EPLF as a tool to analyze the topological properties of non-trivial chemical bonding in molecules.

I. INTRODUCTION

The search for a chemically bound form of tetraoxygen has been the subject of numerous investigations during the last thirty years. Initially, the motivation was given by the analogy with the stable and well-known cyclic and chain forms of sulphur, the study of its fundamental properties and its possible use as a high energy-density material.[1],[2] More recently, it has been proposed as a possible intermediate explaining a variety of experimental findings and appears to have been detected by neutralization reionization (NR) mass spectrometry. Given the different experimental conditions for its preparation and identification, it is important to point out that several forms of tetraoxygen are most likely involved in the different experimental setups, which could include a variety of electronic states and isomers covering a wide range of intermolecular strengths. For example, in the photoionization spectra it has been shown[3],[4] that the O_4 metastable state corresponds to an excited complex between an O_2 molecule in its ground state and another in the excited state, $^1\Sigma_u$. Furthermore, convincing evidence exists that this same species could be involved in the electron transfer to O_4^+ experiments of Helm and Walter[5]. Although these gas phase spectroscopy experiments have suggested the existence of an O_4 species, it is clear that it is not the chemically bound form studied here, but rather electronically excited van der Waals complexes[6],[7],[8]. The same conclusion was drawn in the recent NR mass spectrometric detection of an O_4 species[9].

Most of the complexity found in oxygen-containing species and reactions arises from the unusual electronic structure of molecular oxygen: it has two spin-unpaired electrons occupying degenerate π_g orbitals which lead to a Σ_g^- ground state with a total spin of S=1 and two singlet low-lying excited electronic states. It is therefore not surprising that oxygen, in a variety of forms, exhibits unique properties. For example, while studying the magnetic properties of liquid oxygen, Lewis[10] proposed the formation of an O_4 species to explain the temperature dependence of the magnetic susceptibility emphasizing the failure of Curie's law to describe oxygen, even though the law generally holds for other paramagnetic substances. It is natural to expect the possible formation of an O_4 complex given the radical character of O_2. It is also known that the interaction of two oxygen molecules leads to asymptotically degenerate singlet, triplet and quintet states with stable complexes being bound by weak van der Waals forces[11],[12], [13],[14].

In the solid state, oxygen is the only antiferromagnetic insulating phase among the el-

emental solids and it is the first light element for which metallization was confirmed experimentally. Several solid phases exist at room temperature and high pressures which exhibit a dramatic change of color as the pressure is increased due to changes in the nature of the intermolecular forces, the detailed explanation still being an area of active research [15],[16],[17]. One of the most interesting open problems is the determination and explanation of the structural and optical properties of the ϵ phase which is stable in a broad range of temperatures and high pressures. Some years ago Bini and coworkers[15] measured the infrared spectrum as a function of pressure and noticed the appearance of a new absorption band in the 300-600 cm^{-1} region, in addition to the expected molecular absorption at $\sim$ 1500 cm^{-1}. The new absorption peak was explained through the formation of dimer complexes, O_4, with D_{2h} symmetry analogous to the gas phase van der Waals complex, but the much shorter (30%) intermolecular distances were taken as evidence of a new form of bonding. An alternative theoretical explanation was given by Neaton and Ashcroft[16] who proposed, on the basis of density functional theory, a structure based on linear herringbone-type chains of O_2 molecules consistent with the observed infrared spectra. However, very recently a crystal structure determination has been performed[17] which suggests that the basic unit is composed of 4 molecules, O_8, which interestingly, can be reconciled with the previously proposed structures and explain the optical experiments. In all of the above examples a common theme is the nature of the intermolecular forces binding the molecular oxygen units. A radically different O_4 species has been proposed to exist on the basis of *ab initio* calculations[2],[18] but its experimental detection and characterization is still lacking. The so-called chemically bound O_4 molecule has D_{2d} symmetry with four equivalent single bonds in a cyclic non-planar structure. The bond lengths are similar to those of other oxygen single bonds.

Although it would be natural, given its small number of electrons, to expect that state-of-the-art computational methodologies of quantum chemistry should lead to a full knowledge of the electronic properties of O_4 and its dissociation reaction path to molecular oxygen, this is not the case; a detailed understanding of the chemically bound O_4 molecule still remains a significant quantum theoretical challenge[2],[3], [18],[19],[20], although some important progress has been done very recently[21]. The quantum theoretical difficulties are important and can be briefly stated as follows: the singlet O_4 equilibrium structure has a relatively strong monoreference character, thus it can in principle be calculated by standard and accurate Coupled Cluster (CC) methods. However, describing the transition state of C_2 symmetry leading to dissociation into two triplet oxygen molecules is much more difficult. The open-shell nature of the two diatomic molecules, the description of bond breaking/making processes, and the complicated spin recouplings necessary to describe the transition from four open-shells to a closed shell species can only be properly reproduced with large multiconfigurational wavefunctions. In practice, all along the reaction coordinate the smallest complete active space SCF (CASSCF) wavefunctions have to be built with the three $2p$ shells and the four valence electrons of each atom. This leads to consider 16 elec-

trons within 12 active orbitals [a CASSCF(16,12) calculation], that is to say large CASSCF expansions of 17865 and 70785 configuration state functions (CSF) at the equilibrium and transition state geometries, respectively. On top of that, it is also essential to describe in a *balanced way* the subtle electron-electron interactions, *i.e.* the dynamic correlation effects, arising at the various geometries corresponding to the O_4 reactant, the transition state, and the $O_2(X^3\Sigma_g^-)$+$O_2(X^3\Sigma_g^-)$ products, all of them lying on the lowest singlet potential energy surface.

It is most important to emphasize that obtaining an accurate estimate of the barrier to dissociation is crucial since it determines the stability of the species and, therefore, its relevance for a variety of processes in various phases. Among them, we point out its potential role in atmospheric processes involving ozone and highly vibrationally excited oxygen molecules[22],[23],[24],[25]. The need of an accurate estimation of the heat of formation of this species has already been noted [18], [20]. In a benchmark study using the CCSD(T) and CASSCF(16,12)+ACPF methods with the large aug-cc-pVQZ basis set, it has been found that the heat of formation is significantly smaller and the barrier to dissociation larger ($>$ 9.3kcal/mol) than previously assumed. The same study revealed that the previous theoretical estimate for the heat of formation of tetraoxygen was in error by a significant amount (18-24%) owing to lack of accuracy of the methods then employed for evaluating the correlation energy. Therefore, in a very recent work[21], we have shown that accurate thermochemical values regarding the stability of the O_4 species can be obtained from a totally different but powerful electronic *ab initio* method, namely the quantum Monte Carlo (QMC) approach. MultiReference Fixed-node Diffusion Monte Carlo (MR-FNDMC) calculations were performed to obtain the most accurate dissociation barrier and heat of formation with respect to dissociation into molecular oxygen for the chemically bound tetraoxygen molecule. Multireference trial wavefunctions were used and built from truncated CASSCF(16,12) through a weight-consistent scheme allowing to control the fixed-node error. A favorable comparison with the previous *ab initio* benchmark CASSCF+ACPF/AVQZ results was possible. The MR-FNDMC barrier to dissociation and heat of formation obtained are 11.6$\pm$1.6 kcal/mol and 98.5$\pm$1.9 kcal/mol, respectively. Given the basis-set independence and the excitation-degree free nature of the MR-FNDMC method, these new thermochemical energies should be taken as the theoretical references when discussing the relevance of tetraoxygen in a variety of experiments including the important atmospheric chemical processes where oxygen species play a fundamental role.

Given that for the $O_4 \leftrightarrows O_2(X^3\Sigma_g^-)$+$O_2(X^3\Sigma_g^-)$ reaction the main problem found with standard *ab initio* methods for the accurate evaluation of the reaction barrier is the need to accurately deal with the dynamic correlation effects (on top of the strongly multiconfigurational wavefunction) at the transition state geometry, it would seem that the electronic distributions of the bonds around the four oxygen nuclei strongly depend on the method used to describe it. We note that, even at the equilibrium geometry of the O_4 molecule, the CASSCF wavefunction contains 24 determinants with a coefficient larger than 0.05 (see,

Table I).

Although ground-state energies are of primary interest, it is clear that a chemical understanding of a complex molecular system requires more than the knowledge of the sole ground-state energy. In general, chemists are interested in rationalizing and quantifying the structure and reactivity of the system in terms of various quantities related to electron localization. A number of important questions we wish to answer here include, for example, the nature of the bonding between atoms, the localization of lone pairs, and the local concentration or depletion of charge at the two important critical points of the PES of the $O_4 \leftrightarrows 2O_2$ reaction. In standard computational chemistry several approaches have been developed to analyze and visualize the electronic distribution in the ordinary 3D-space. Among them we can cite, *e.g.*, the methods analyzing the deformation of densities (a build-up of charge between two atoms is interpreted as the existence of a bond)[26], the methods based on the topological analysis of the electron density or its Laplacian (see, for instance, Bader [27]), the methods studying the topography of the molecular electrostatic field[28] and, also, approaches using as indicator the electron localization function (ELF) describing the amount of local Pauli repulsion between electrons[29],[30]. Of course, this list cannot be considered as exhaustive since defining a successful and general qualitative model for the description of chemical structure is an everlasting theme in chemistry since the pioneering electron-pair model of Lewis.

In this work we propose to exploit the accurate data obtained from quantum Monte Carlo simulations on the $O_4 \leftrightarrows 2O_2$ reaction to get important insights into the electron localization properties of the tetraoxygen molecule at its equilibirum geometry and at the transition state leading to two ground state oxygen molecules. To do that we shall use the function, introduced by some of us recently [31], describing the pairing of electrons in a molecular system. This function, called Electron Pair Localization Function (EPLF), is built to reveal the differences in the average distances between spin-like and spin-unlike electrons. In regions where localized pairs of electrons are present (lone pairs, atomic pairs, bonds) the EPLF takes large values and displays maxima. In contrast, in regions where electrons behave essentially as an homogeneous fluid (spin-like and spin-unlike electrons being mixed together), the EPLF takes much smaller values. The form of the EPLF is simple (see next section) and has been chosen to be easily computable using quantum Monte Carlo (QMC) calculations. A major advantage of QMC is the possibility of evaluating the EPLF at various levels of accuracy (Hartree-Fock, Multiconfigurational SCF, Valence Bond, DFT, Variational Monte Carlo with explicitly correlated trial wave functions, fixed-node Diffusion MC, etc.. . .).

Originally applied to several simple atomic and molecular systems[31], the EPLF appears to be a practical tool for describing electronic features in more complex molecular systems[32]. We shall apply it here to a much more challenging chemical problem, the $O_4 \leftrightarrows O_2(X^3\Sigma_g^-)+O_2(X^3\Sigma_g^-)$ reaction. The organization of the paper is as follows: in Sec. II the basic features of QMC needed to understand the present work are briefly presented.

In particular, we summarize the various probability densities produced by QMC. Section III is a very brief review of the electron pair localization function (EPLF). Section IV presents the results and analysis of the EPLF using various types of electronic structure methods at different geometries (equilibrium, transition state, and along the reaction coordinate connecting the transition state and the two dissociated molecules). Finally, in Section V a summary of the main results is presented.

II. QUANTUM MONTE CARLO

In a quantum Monte Carlo scheme a series of "states" or "configurations" are generated using some elementary stochastic rules. Here, a configuration is defined as the set of the $3N$-electronic coordinates (N number of electrons), the positions of the nuclei being fixed (Born-Oppenheimer condition)

$$\vec{R} = (\vec{r_1}, \ldots, \vec{r_N}). \tag{1}$$

Stated differently, a configuration $\vec{R}$ may be viewed as a "snapshot" of the molecule showing the instantaneous positions of each electron. Stochastic rules are chosen so that configurations are generated according to some target probability density, $\Pi(\vec{R})$. Note that the probability density is defined over the complete $3N$-dimensional configuration space and not over the ordinary 3D-space. Many variants of QMC can be found in the literature (referred to with various acronyms: VMC, DMC, PDMC, GFMC, etc...). They essentially differ by the type of stochastic rules used and/or by the specific stationary density produced. In practice, the two most popular QMC approaches used for simulating complex molecular systems are the so-called Variational Monte Carlo (VMC) and fixed-node Diffusion Monte Carlo (FN-DMC) methods. Both methods will be employed here. Let us briefly summarize the basic features of these methods useful for the following (for a detailed presentation, see, *e.g.*, [33]).

A. Variational Monte Carlo (VMC)

In a VMC calculation the probability density generated is given by

$$\Pi_{VMC}(\vec{R}) = {\psi_T}^2(\vec{R}) \tag{2}$$

where ψ_T is a high-quality electronic trial wave function. A commonly used expression for ψ_T consists of a product of two terms. The first term is standard and is introduced to describe the one-particle shell-structure of molecules. It is obtained from a preliminary HF or DFT *ab initio* calculation and is expressed as one (or a combination of a few) determinant(s) of single-particle spatial orbitals. The second term is introduced to reproduce the electron-electron cusp condition of the exact wave function and, also, to incorporate some explicit coupling between electron-nucleus and electron-electron coordinates (see, [34]). Note that

the electron-electron cusp condition is known to be particularly difficult to fulfill in standard *ab initio* calculations using expansions over one-electron basis sets (necessity of considering very high values of the orbital momentum). The explicitly correlated term is usually referred to as the Jastrow factor. In a spin-free formalism our trial wave function is written as

$$\psi_T(\vec{R}) = D^{\uparrow}(\vec{R}) D^{\downarrow}(\vec{R}) \exp\left[\sum_{\alpha} \sum_{\langle i,j \rangle} U(r_{i\alpha}, r_{j\alpha}, r_{ij})\right] \tag{3}$$

where the sum over α denotes a sum over the nuclei, $\sum_{\langle i,j \rangle}$ a sum over the pair of electrons, and $D^{\sigma}(\sigma = \uparrow \text{ or } \downarrow)$ are determinants made of one-particle space-orbitals. Different expressions for the Jastrow part have been presented in the literature. Here, we have chosen the following form[35]

$$U(r_{i\alpha}, r_{j\alpha}, r_{ij}) =$$
$$s(x_{ij}) + p^{(\alpha)}(x_{i\alpha}) + c_1 x_{i\alpha}^2 x_{j\alpha}^2 + c_2 (x_{i\alpha}^2 + x_{j\alpha}^2) x_{ij}^2 + c_3 x_{ij}^2 \tag{4}$$

with

$$x_{ij} = \frac{r_{ij}}{1 + b_{\sigma} r_{ij}}$$
$$x_{i\alpha} = \frac{r_{i\alpha}}{1 + b_{\alpha} r_{i\alpha}}$$
$$s(x) = s_1 x + s_2 x^2 + s_3 x^3 + s_4 x^4$$
$$p^{(\alpha)}(x) = p_1^{(\alpha)} x + p_2^{(\alpha)} x^2 + p_3^{(\alpha)} x^3 + p_4^{(\alpha)} x^4,$$

b_{σ} can take two different values depending on the spin of the pairs of electrons considered. In this latter expression the quantities $\{b_{\sigma},\, b_{\alpha},\, c_i,\, s_i,\, p_i^{(\alpha)}\}$ play the role of parameters.

The critical step in a VMC approach is the optimization of the parameters entering the trial wave function. A standard method consists in searching for parameters minimizing the fluctuations in configuration space of the local energy defined as

$$E_L(\vec{R}) \equiv H\Psi_T / \Psi_T. \tag{5}$$

This criterion is based on the fact that for the exact wave function the local energy reduces everywhere to a constant -the exact energy- and, thus, the fluctuations of the local energy entirely vanish. Accordingly, small fluctuations are associated with "good" trial wave functions. A number of methods have been developed to perform efficiently the optimization step within a QMC framework. In this work, we have used the correlated sampling method of Umrigar *et al.*[36], an approach based on the minimization of the weighted variance of the local energy over a set of fixed configurations.

Once the optimal parameters have been determined, the quality of the resulting trial wave function is usually good. A major part of the dynamical correlation energy (Coulomb hole) is recovered and the *gross* features of the one-particle background are also correctly described via the determinantal part (i.e. the non-dynamical correlation). For most atoms

it is possible to recover up to $80\% - 90\%$ of the exact correlation energy[34]; for molecules the domain of variation lies usually between 30 and 90%.

The numerical method (stochastic rules) employed to generate the VMC density, Eq.(2), is standard. It is based on the use of an improved Metropolis algorithm[37].

B. Diffusion Monte Carlo (DMC)

In a diffusion Monte Carlo scheme the stochastic rules employed are the same as in the VMC case (Metropolis algorithm) plus a new rule corresponding to a branching (or birth-death) process. More precisely, depending on the magnitude of the local energy a given configuration is destroyed (when the local energy is greater than some estimate of the exact energy) or duplicated a certain number of times (local energy lower than the exact energy). It can be shown that the stationary density resulting from these rules is now given by

$$\Pi_{DMC}(\vec{R}) = \psi_T(\vec{R})\phi_0(\vec{R}) \tag{6}$$

where $\phi_0(\vec{R})$ denotes the ground-state wave function.

Fixed-node error. Actually, because the density Π_{DMC} is necessarily positive, as any stationary density resulting from some stochastic rules, ϕ_0 is not the exact ground-state wave function, but some approximate one resulting from the additional constraint that ϕ_0 must have the same sign as the trial wave function so that the product in Eq.(6) is always positive. In other words, the mathematical eigenproblem solved is not the exact one but, rather, some modified one which can be written as

$$H\phi_0^{FN}(\vec{R}) = E_0^{FN}\phi_0^{FN}(\vec{R}) \tag{7}$$

where $\phi_0^{FN}(\vec{R}) = 0$ whenever $\psi_T(\vec{R}) = 0$.

The fact that the nodes (points in $3N$-dimensional space where the wave function vanishes) of ψ_T and ϕ_0^{FN} are identical leads to a so-called "fixed-node" error. However, as far as total energies are concerned, this approximation is in general very good and the fixed-node error on total energies represents usually a small fraction of the total correlation energy. Let us emphasize that this error depends only on the quality of the nodes; see, *e.g.*, the discussion in [38]).

C. Multireference Fixed-Node Diffusion Monte Carlo (MR-FN-DMC)

We have recently shown that for the problem we are interested in here, the thermochemical quantities obtained with FN-DMC (reaction barrier and dissociation energy) are very badly reproduced when the single-reference Hartee-Fock nodes are used, both for the equilibrium and for the transition-state geometries.[21] Since the most critical quantity relevant for the determination of the feasibility of the experimental detection of gas-phase O_4 is the

reaction barrier, we focused our attention on these two critical points of the O_4 singlet PES. To get a coherent description of the nodal patterns at both geometries we proposed a scheme based on the study of the fixed-node error evolution for both structures, as a function of the size of a truncated expansion of the large CASSCF(16,12) wavefunction used as DMC trial wavefunction. Note that the basis set employed here is the large aug-cc-pVTZ basis set. The truncation is simply done by choosing the configurations within the CASSCF expansion that have a coefficient larger than a given threshold ϵ, thus defining a set MR(ϵ) at each geometry

$$\Psi_{MR}(\vec{R}) = \sum_{i \in MR(\epsilon)} c_i \phi_i(\vec{R}). \tag{8}$$

The full trial wavefunction is thus written as

$$\psi_T(\vec{R}) = \Psi_{MR}(\vec{R}) \exp\left[\sum_{\alpha} \sum_{\langle i,j \rangle} U(r_{i\alpha}, r_{j\alpha}, r_{ij})\right]. \tag{9}$$

In this work, we consider that the Fixed-Node DMC energy difference obtained is meaningful only when the two following conditions are fulfilled. First, the energy difference as a function of decreasing values of ϵ must be found almost constant within statistical fluctuations. Second, the nodal error must display some "robustness" with respect to dynamical correlation effects. By this, it is meant that the nodal patterns must not change significantly under re-optimization (energy minimization) of the coefficients of the truncated expansion c_i in the presence of the Jastrow factor.

¿From a theoretical point of view, this procedure is based on the assumption that the nodal pattern of the exact wavefunction can be correctly described by considering *separetely* the non-dynamical correlation effects (CASSCF part) and the dynamical ones (Jastrow part). Clearly, this "first-order" approximation is natural but is not expected to be valid for all molecular systems.

III. THE ELECTRON PAIR LOCALIZATION FUNCTION (EPLF)

Let us briefly present the electron pair localization function (EPLF). The EPLF is a local scalar function defined in the ordinary 3D-space, bounded above and below, which focuses essentially on the localization of electron *pairs*. It is a good descriptive tool for chemical bonds, since pairs of electrons play a central role in our everyday interpretation of chemical structure and reactivity (Lewis model, VSEPR). The framework proposed to calculate such a localization function is that of quantum Monte Carlo approaches. As emphasized in the introduction, QMC are techniques of a great versatility and, therefore, the definition of the EPLF proposed below will be of practical use for any type of wavefunctions (HF, post-HF, Valence Bond, etc...) and for any level of computation (VMC, FN-DMC,"exact").

First, we need to introduce the two local quantities $d_{\sigma\sigma}(\vec{r})$ and $d_{\sigma\bar{\sigma}}(\vec{r})$ defined as follows

$$d_{\sigma\sigma}(\vec{r}) \equiv \sum_{i=1}^{N} \langle\langle \delta(\vec{r}-\vec{r}_i) \min_{j;\ \sigma_j=\sigma_i} |\vec{r}_i - \vec{r}_j| \rangle\rangle$$

$$d_{\sigma\bar{\sigma}}(\vec{r}) \equiv \sum_{i=1}^{N} \langle\langle \delta(\vec{r}-\vec{r}_i) \min_{j;\ \sigma_j\neq\sigma_i} |\vec{r}_i - \vec{r}_j| \rangle\rangle \tag{10}$$

where $\{\vec{r}_k\}_{k=1,N}$ are the positions of the N electrons for a given configuration $\vec{R}$, σ_i is the spin of the i^{th} electron ($\sigma_i = \uparrow, \downarrow$), and $\langle\langle ... \rangle\rangle$ the stochastic average over the Monte Carlo configurations. As seen from these definitions $d_{\sigma\sigma}(\vec{r})$ [resp., $d_{\sigma\bar{\sigma}}(\vec{r})$] is the average distance between an electron located at $\vec{r}$ and the closest spin-like (resp., spin-unlike) electron of the molecule.

The electron pair localization function (EPLF) is defined as

$$\mathrm{EPLF}(\vec{r}) = \frac{d_{\sigma\sigma}(\vec{r}) - d_{\sigma\bar{\sigma}}(\vec{r})}{d_{\sigma\sigma}(\vec{r}) + d_{\sigma\bar{\sigma}}(\vec{r})} \tag{11}$$

Figure 1 of [31] gives a simple pictorial representation of the construction of the EPLF in the case of only one configuration and four electrons in 2D.

By definition the EPLF takes its values within the interval [-1,1]. It gives a local indicator of electron pairing as follows. In regions of space where electrons are unpaired the average distances between spin-like and spin-unlike electrons are similar, $d_{\sigma\bar{\sigma}} \approx d_{\sigma\sigma}$, and the EPLF goes to zero. When spin-unlike electrons are paired we have $d_{\sigma\bar{\sigma}} \ll d_{\sigma\sigma}$ and EPLF goes to 1. Finally, when spin-like electrons are paired, $d_{\sigma\bar{\sigma}} \gg d_{\sigma\sigma}$ and, thus, EPLF goes to -1. The EPLF main feature is to reveal the differences in the average distances between spin-like and spin-unlike electrons. In regions where localized pairs of electrons are present (lone pairs, atomic pairs, bonds) the EPLF takes larger values and displays maxima. In contrast, in regions where electrons behave essentially as an homogeneous fluid (spin-like and spin-unlike electrons being mixed together), the EPLF takes much smaller values. In particular note that for molecules with one or more open shells as is the case with molecular oxygen here, in regions where there is a larger amount spin-up (or spin-down) density, by construction the EPLF takes on minima values. Note that the definition of EPLF is particularly well suited to QMC; the formula (10) can indeed be easily computed with any QMC scheme.

IV. COMPUTATIONAL DETAILS

Trial wave functions. The oxygen basis set used is the fully decontracted Dunning aug-cc-pVTZ basis set[39] and the optimized geometries chosen for the O_4 reactant and the transition state are those previously determined at the multireference Rayleigh-Schrödinger perturbed Second-Order (CASSCF-RS2) level, which are the most accurate ones to date. The determination of the critical points of the singlet potential energy surface was done

through benchmark-type CASSCF-RS2 calculations with a very large monoelectronic basis of 320 molecular orbitals and taking into account up to 5.1×10^{10} CSF [20]. The trial wavefunctions used here consist of the truncated CASSCF(16,12) determinantal expansion discussed above multiplied by a standard Jastrow prefactor taking into account the explicit electron-electron and electron-electron-nucleus interactions (see, e.g. [40],[41]). Note that for a system consisting of light atoms such as O_4 some care has to be taken for properly reproducing the electron-nucleus cusp both for the core and valence electrons. Regarding the core region, we have replaced the four $1s$ atomic orbitals expanded over the gaussian basis set by the $1s$ Slater-type orbital given in the Clementi and Roetti's Tables [42]. On the other hand, the valence molecular orbitals are also modified at short nuclear distances to impose the nuclear cusp; we do that using a short-r representation of the radial part of orbitals under the form $c_1 \exp(-\gamma_1 r) + c_2 r^2 exp(-\gamma_2 r)$, in the same spirit as Ref.[43]. The present FN-DMC calculations are all-electron calculations done with a very small time-step, $\tau = 0.00015$, to insure a proper treatment of the nodal hypersurfaces and to reduce time-step errors. For each trial wave function, the calculations are not extensive and represent only about 10^7 Monte Carlo steps distributed over 20 processors. Since the EPLF gives only qualitative information, the number of steps needed to obtain relevant results is much smaller than the number of steps needed to get an acceptable error bar for the energy. Moreover, it should be stressed that, in sharp contrast with the energy, the quality of the trial wave function has little impact on the magnitude of the statistical error on the EPLF results, since the quantities which are averaged during the Monte Carlo simulation, Eq.(10), are not a function of the trial wavefunction.

In the case of the multireference trial wavefunctions, we have used the same wavefunctions as the largest reported in [21] with a cutoff CI coefficient of 0.05 in the CASSCF expansions at both (the TS and product) geometries, leading to 24 and 14 CSF for the equilibrium product and TS geometries, respectively. These wavefunctions are used to represent the determinantal part of the trial functions used in the quantum Monte Carlo computations.

QMC data. The densities relative to HF wave functions, Eq.(2), have been sampled by Variational Monte Carlo simulations (VMC) and are labeled HF-VMC. The densities relative to the truncated CASSCF wave functions which have been sampled by Variational Monte Carlo simulations (VMC) and are labeled MR-VMC. The densities relative to truncated CASSCF wave functions which have been sampled by multireference fixed-node diffusion Monte Carlo simulations are labeled MR-FNDMC.

The trial wave functions have also been improved by introducing an explicitly correlated Jastrow factor as described above, Eq.(4). The density corresponding to these wavefunctions have been sampled by VMC, labeled Jast-VMC.

For each geometry considered, a typical simulation includes a set of 800 independent walkers and a number of Monte Carlo steps per walker of about 100000.

EPLF data. The continuous 3D-space is represented using a $80 \times 80 \times 80$ three-dimensional grid. The EPLF is calculated as follows: for each Monte Carlo configuration generated the

positions of the electrons are scanned. The elementary volume of the 3D-grid occupied by each electron is determined and the minimum distances appearing in the definition of EPLF are calculated. The noise in the localization function due to the statistical character of QMC simulations has been reduced by using a median blur filter as detailed in Ref.[31]. This filter is particular well adapted here since it is known to modify very little the regions where the gradient is large. This latter point is particularly important here since we are interested in altering as little as possible the contours of the pair localization function.

V. RESULTS: THE EPLF

As we shall see below, the topology of the EPLF for the various systems and geometries presented here are found to be sensitive to non-dynamical correlation (introduced via CASSCF expansions) but much less to dynamical correlation (via explicitly correlated Jastrow factors and/or DMC simulations). Accordingly, to keep the number of figures shown reasonable, only the EPLF figures obtained from calculations done at the Hartree-Fock and truncated CASSCF(16,12) levels are presented.

A. The O_4 equilibrium geometry

In Figs. 1 and 2 we present the 3D-plots for the EPLF at a given isosurface value obtained with the Hartree-Fock (EPLF=0.10) and the truncated CASSCF(16,12) wave functions (EPLF=0.11), respectively. The EPLF topology in both cases is very similar and lead to a clear chemical picture. As seen from these figures, the EPLF reveals the atomic shell structure: one small spherical domain around each oxygen nucleus corresponding to the $1s$ electron pairs and two separate domains on each oxygen corresponding to the lone pairs. Regarding the bonding pattern, four disk-shaped domains corresponding to four equivalent σ bonds are observed, these domains being exactly located at the midpoints of the four internuclear oxygen-oxygen axes. Also clearly visible is the local tetrahedral structure around each oxygen atom between its two lone pairs and the two covalent bonds formed with the two closest neighbors (sp^3 hybridization). Note that the optimized interoxygen distances in this molecule are very close to other oxygen-oxygen distances corresponding to single bonds[20].

B. The ground state triplet oxygen molecule

For the triplet oxygen molecule the ROHF and the CASSCF valence wavefunctions are almost identical and can be well described (in second-quantized notation) as a single $|222{+}{+}\rangle$ determinant, where the last two are degenerate π molecular orbitals. One can relate the electronic structure of the O_2 triplet ground state with that of the singlet ground state of N_2 by noting that the orbital occupation ordering of the former can be obtained by putting

the couple of extra electrons in triplet coupling (i.e. unpaired spins), one in each of the degenerate π orbitals, which are virtual orbitals in the latter case. Therefore, using the same second-quantized notation for the HF or CASSCF valence wavefunction of the singlet ground state of N_2 can be written as as a single $|222\rangle$ determinant. Given that for large values the EPLF shows electron pairings and that, for low values, the EPLF shows regions where spin-unpaired electrons are found, it is natural to ask if the EPLF of the O_2 molecule in its triplet ground state resembles that of N_2. To test this idea we have calculated the EPLF for the ground states of O_2 and N_2 using their HF/6-311G* wavefunctions. To show regions where electrons are paired we plot the surfaces where the EPLF has values larger than +0.1 (vrfier Anthony) [44], in Figure 3 for N_2 and in Figure 4 for O_2. According to the above mentioned wavefunction composition, there are two maxima for the regions of the doubly occupied p orbital and an infinite number of minima on a torus, see Figure 4. Note that the central "pancake-like" domain found at the midpoint along the internuclear axis corresponds to a an axial σ bond superimposed on the two orthogonal π bonds which lead to maxima on a torus surrounding the axial bond. The outer lone pair domains appear in axial configuration for both molecules. Clearly, the EPLF isosurfaces for large values are qualitatively identical in both molecules. Conversely, to show regions where electrons are unpaired we show the volumes where the absolute value of the EPLF is larger than 0.03 (vrfier Anthony) in Figure 5 for N_2 and in Figure 6 for O_2. In this case the volume contained by the toroidal isosurface for N_2 has no electrons and it contains roughly 2 same-spin electrons in the O_2 case. With the understanding of the topology of the EPLF for the separate O_2 fragments, we can now proceed to the analysis of the bond-breaking and bond-making process along the reaction coordinate.

C. The Transition State system

The analysis of the EPLF at the transition state (TS) turns out to be a much more challenging task. The EPLF at the TS is given in Figure **??** at the HF level and in Figure **??** at the CASSCF level using a truncation threshold of $c_i > 0.05$. One could naïvely think that the identification of the bond-forming and bond-breaking processes of this reaction is a straightforward matter which could be simply done by analyzing the evolution of the wavefunction along the reaction coordinate. For the HF case it could theoretically be done in terms of the HF canonical orbitals, while for the truncated CASSCF case this could be achieved in terms of the natural orbitals and the configuration state functions (CSF). However, the presence of a large number of configurations, both at the O_4 equilibrium geometry and at the transition state, casts serious doubts on the validity of the HF description of this complex reaction. In practice, the identification of the bond-forming and bond-breaking processes is quite a tough and tedious task. In particular, an important necessary step is to localize the molecular orbitals, a task for which there does not exist a general criterium-free

scheme and for which some fragment reference is needed. Given the equivalence of the four oxygen atoms along the reaction coordinate close to the TS, there is a practical problem to define coherently the reference fragments on both the negative (towards O_4) and the positive (towards two O_2 molecules) reaction coordinate. We highlight that for the truncated CASSCF the situation is even more difficult than in the HF case, because of the strongly multiconfigurational character of the wavefunction; this point is clearly illustrated in table II where the coefficients of the CSF whose magnitude is greater than 0.05 are presented.

D. Bond-forming/Bond-breaking

To understand bond-forming and bond-breaking processes from the TS towards the isolated oxygen molecules, we have performed CASSCF calculations at several (equally spaced) geometries following the positive reaction coordinate as given in figure 4a of [18] up to 6 units; see that reference for a precise definition of this reaction distance. In Figure **??** the EPLF isosurfaces are plotted for every geometry used along the dissociation path for a value of 0.10. This series of snapshots show the strikingly complex synchronous intermolecular bond-breaking and intramolecular bond-making processes that lead to bimolecular dissociation. Although difficult to perceive with a single planar perspective, we note that the topology of the EPLF at the TS geometry is perfectly symmetrical as seen from any of the four equivalent oxygen-oxygen midpoints; thus, to facilitate the analysis, in this figure we have highlighted in red the O-O internuclear axes of the final O_2 fragments. In particular, we note three sequential outstanding facts: a) the narrow bridges connecting the (different fragments) lone pair domains in the TS are the first to be broken (the upper three snapshots); b) then the domains that connect the two dissociating O_2 moieties are broken one after the other (rightmost upper to middle central snapshots); c) finally, the couple of separate lone pair domains around each oxygen atom get thinner and fuse to form the single axial domain (two at both ends of each O_2 molecule) of the dissociated fragments. Thus the EPLF analysis has allowed us to find the sequence of topological transformations of the electron pairings are at the root of an overall decrease of more than 90kcal/mol from the TS singlet configuration to the separate couple of O_2 triplet fragments [18].

Although not shown here, we have obtained the EPLF surfaces following the same positive reaction coordinate using as wavefunction a single HF determinant. An important and somewhat unexpected result is that the qualitative bond-forming and bond-breaking picture is the same as that obtained using the CASSCF wavefunction. Thus for this interpretation, unlike what was found for the energy barrier, the zeroth-order description provided by the HF approximation seems to be enough.

Clearly, this interpretation could not have been extracted just by looking at the CSF composition of the truncated CASSCF wavefunction of the transition state as given in table II and its evolution along the reaction coordinate. Finally, we stress that the introduction

of the explicit interelectronic Jastrow prefactor has been found here of little importance to address the evolution of electron pairing along the reaction coordinate. This is actually not surprising since the very strong multiconfigurational nature of the wavefunction is clearly the dominant feature. To introduce or not the Jastrow term can *a priori* be expected to be less important than the use of a zeroth-order MCSCF description. At this point it is interesting to note that the total energy calculated with the Jastrow term is slightly lower than the truncated CASSCF(16,12) one. The short-range Jastrow factor allows the electrons to better avoid each other locally, thus significantly diminishing the single-reference energy; however, the truncated CASSCF(16,12) description, which is diabatically correlated with the bimolecular dissociation fragments (ground state molecular oxygen), is more physical as shown by recent extensive MR-FNDMC calculations[21].

VI. SUMMARY

In this paper we have used the electron pair localization function (EPLF) to study the electronic pairing distribution at two particularly important critical points of the potential energy surface of the $O_4 \leftrightarrows 2O_2$ reaction. At the equilibrium geometry of O_4 the EPLF reveals four equivalent covalent bonds and a couple of lone pairs surrounding each oxygen atom. This is true for all levels of theory. At the transition state geometry the EPLF allowed us to obtain a detailed understanding of the electronic structure at different levels of theory; in particular at the truncated CASSCF level, which provides the correct zeroth-order electronic description, the EPLF revealed the superposition of triplet oxygen atom on top of the EPLF of the isolated O_3 entity. This picture is consistent with two unpaired electrons (α,α or β,β) on the oxygen atom and two unpaired electrons (β,β or α,α) on the O_3 fragment.

¿From a more general perspective, we would like to emphasize the usefulness of EPLF which is both simple and easily computable using quantum Monte Carlo. A major advantage of QMC is the possibility of evaluating the EPLF at various levels of accuracy (Hartree-Fock, MCSCF, VB, DFT, Variational Monte Carlo with explicitly correlated trial wave functions, fixed-node DMC, etc...). Such a possibility is particularly interesting to get new insights into the nature of the pairing and localization of electrons at these various levels of description and, particularly, to understand more deeply the role of the dynamical (Coulomb hole) and the non-dynamical (near-degeneracy) correlation effects.

Acknowledgments MC and AS would like to thank IDRIS (CNRS, Orsay), CCRT (CEA/DAM, Ile-de-France), CALMIP (Université de Toulouse) for computational support. ARS wishes to thank the FOMES2000 "Cómputo Científico" Project for CPU time on the IBM-p690 supercomputer and support from CONACYT project number 45986-E. ARS also

thanks unlimited CPU time on the CNSI facility at UC Santa Barbara.

---

[1] V. Adamantides, D. Neisius, G. Verhaegen, Chem. Phys. **48**, 215 (1980).

[2] E.T. Seidl, H.F. Schaefer, J. Chem. Phys. **96**, 1176 (1992).

[3] D.S. Peterka, M. Ahmed, A.G. Suits, K.J. Wilson, A. Korkin, M. Nooijen, R.J. Bartlett, J. Chem. Phys.**110**, 6095 (1999).

[4] D.S. Peterka, M. Ahmed, A.G. Suits, K.J. Wilson, A. Korkin, M. Nooijen, R.J. Bartlett, J. Chem. Phys.**111**, 5279 (1999);

[5] H. Helm, C. W. Walter, J. Chem. Phys. **98**, 544 (1993).

[6] C.A. Long, G.E. Ewing, J. Chem. Phys. **58**, 4824 (1973).

[7] J. Goodman, L. E. Brus, J. Chem. Phys. **67**, 4398 (1977).

[8] P. E. S. Wormer, A. van der Avoird, J. Chem. Phys. **81**, 1929 (1984).

[9] F. Cacace, G. de Petris, A. Troiani, Angew. Chem. Int. Ed. **40**, 4062 (2001).

[10] G.N. Lewis, J. Am. Chem. Soc. **46**, 2027 (1924).

[11] B. Bussery , P.E.S. Wormer, J. Chem. Phys. **99**, 1230 (1993).

[12] V. Aquilanti, D. Ascenzi, M. Bartolomei, D. Cappelletti, S. Cavalli, M. de Castro Vitores, F. Pirani, Phys. Rev. Lett. **82**, 69i (1999).

[13] V. Aquilanti, D. Ascenzi, M. Bartolomei, D. Cappelletti, S. Cavalli, M. de Castro Vitores, F. Pirani, J. Am. Chem. Soc. **121**, 10794 (1999).

[14] R. Hernández-Lamoneda, M. Bartolomei, M.I. Hernández, J. Campos-Martínez, F. Dayou, J. Phys. Chem. A **109**, 11587 (2005).

[15] F. A. Gorelli, L. Ulivi, M. Santoro, R. Bini, Phys. Rev. Lett. **83**, 4093 (1999).

[16] J. B. Neaton, N. W. Ashcroft, Phys. Rev. Lett. **88**, 205503 (2002).

[17] H. Fujihisa, Y. Akahama, H. Kawamura, Y. Ohishi, O. Shimomura, H.Yamawaki, M. Sakashita, Y. Gotoh, S. Takeya, K. Honda, Phys. Rev. Lett. **97**, 085503 (2006).

[18] R. Hernández-Lamoneda, A. Ramírez-Solís, J. Chem. Phys. **113**, 4139 (2000).

[19] D. Schröder, Angew. Chem. Int. Ed. Engl. **41**, 573 (2002).

[20] R. Hernández-Lamoneda, A. Ramírez-Solís, J. Chem. Phys. **120**, 10084 (2004).

[21] M. Caffarel, A. Scemama, R. Hernández-Lamoneda and A. Ramírez-Solís, Phys. Rev. Lett. **99**, 153001 (2007).

[22] H. Park and T. G. Slanger, J. Chem. Phys. **100**, 287 (1994).

[23] R. Hernández, R. Toumi, D.C. Clary, J. Chem. Phys. **102**, 9544 (1995).

[24] R. L. Miller, A. G. Suits, P. L. Houston, R. Toumi, J. A. Mack, A. M. Wodtke, Science **265**, 1831 (1994).

[25] D.M. Lauvergnat, D.C. Clary, J. Chem. Phys. **108**, 3566 (1998).

[26] P. Coppens and M. B. Hall (Eds.). *Electron Distributions and Chemical Bonds*. Plenum, New York, 1982.

[27] R. F. W. Bader. *Atoms in Molecules: A Quantum Theory*. Clarendon, Oxford, 1990.

[28] S. R. Gadre, S. A. Kulkarni, and I. H. Shrivastava. *J. Chem. Phys.*, 96, 5253, 1992.

[29] A. D. Becke and K. E. Edgecombe. *J. Chem. Phys.*, 92, 5397, 1990.

[30] B. Silvi and A. Savin. *Nature*, 371:683–686, 1994.

[31] A. Scemama, P. Chaquin and M. Caffarel, J. Chem. Phys. **121**, 1725 (2004).

[32] C. Amador-Bedolla, R. Salomón-Ferrer, W.A. Lester, J.A. Vázquez-Martínez and A. Aspuru-Guzik, J. Chem. Phys. **126**, 204308 (2007).

[33] B.L. Hammond, W.A. Lester Jr., and P.J. Reynolds, *Monte Carlo Methods in Ab Initio Quantum Chemistry*, World Scientific Lecture and Course Notes in Chemistry Vol.1 (1994).

[34] K. E. Schmidt and J. W. Moskowitz. *J. Chem. Phys.*, 93, 4172, 1990.

[35] R. Assaraf and M. Caffarel. *J. Chem. Phys.*, 113:4028, 2000.

[36] C. J. Umrigar, K. G. Wilson, and J. W. Wilkins. *Phys. Rev. Lett.*, 60, 1709, 1988.

[37] A. Scemama, T. Lelièvre, G. Stoltz, E. Cancès and M. Caffarel. *J. Chem. Phys.*, 125, 114105, 2006.

[38] H. J. Flad, M. Caffarel, and A. Savin. *Recent Advances in Quantum Monte Carlo Methods*. World scientific publishing edition, 1997.

[39] T. H. Dunning. *J. Chem. Phys.*, 90, 1007, 1989.

[40] R. Assaraf and M. Caffarel, J. Chem. Phys. **113**, 4028 (2000).

[41] C. Filippi and C.J. Umrigar, J. Chem. Phys. **105**, 213 (1996).

[42] E. Clementi and C. Roetti, Atomic Data and Nuclear Data Tables **14** 177 (1974);

[43] S. Manten and A. Lüchow, J. Chem. Phys. **115**, 5362 (2001).

[44] In order place in the correct context this threshold, it is important to know that the largest value of the EPLF are xxx and yyy for O_2 and N_2

Configuration	Coefficient c_i
$\mid a_1$: 2220 a_2: 220 b_1: 220 b_2: 20$\rangle$	0.9081534
$\mid a_1$: 2220 a_2: 202 b_1: 220 b_2: 20$\rangle$	-0.0749640
$\mid a_1$: 2220 a_2: 220 b_1: 220 b_2: 02$\rangle$	-0.0661446
$\mid a_1$: 2220 a_2: 220 b_1: 2-+ b_2: +-$\rangle$	-0.0600672
$\mid a_1$: 2220 a_2: 220 b_1: 2+- b_2: -+$\rangle$	-0.0600672
$\mid a_1$: 2220 a_2: 220 b_1: 2- - b_2: ++$\rangle$	0.0598511
$\mid a_1$: 2220 a_2: 220 b_1: 2++ b_2: - -$\rangle$	0.0598511
$\mid a_1$: 2220 a_2: 2-+ b_1: 220 b_2: +-$\rangle$	0.0580685
$\mid a_1$: 2220 a_2: 2+- b_1: 220 b_2: -+$\rangle$	0.0580685
$\mid a_1$: 2220 a_2: 2- - b_1: 220 b_2: ++$\rangle$	-0.0577911
$\mid a_1$: 2220 a_2: 2++ b_1: 220 b_2: - -$\rangle$	-0.0577911
$\mid a_1$: 2220 a_2: 220 b_1: 222 b_2: 00$\rangle$	-0.0574860
$\mid a_1$: 2220 a_2: 222 b_1: 220 b_2: 00$\rangle$	-0.0574154
$\mid a_1$: 2022 a_2: 220 b_1: 220 b_2: 20$\rangle$	-0.0523990
$\mid a_1$: 2+2- a_2: 220 b_1: 2-+ b_2: 20$\rangle$	0.0510929
$\mid a_1$: 2-2+ a_2: 220 b_1: 2+- b_2: 20$\rangle$	0.0510929
$\mid a_1$: 2220 a_2: 2-+ b_1: 2+- b_2: 20$\rangle$	-0.0509593
$\mid a_1$: 2220 a_2: 2+- b_1: 2-+ b_2: 20$\rangle$	-0.0509593
$\mid a_1$: 2220 a_2: 220 b_1: 200 b_2: 22$\rangle$	-0.0504427

TABLE I: CASSCF wavefunction of O_4 at equilibrium geometry, $\Psi = \sum_i c_i \mid ...\rangle$. All coefficients c_i having a modulus greater than 0.05 are given. Second quantized notation, see text. Molecular orbitals grouped according to their symmetry (using the a_1, a_2, b_1, and b_2 irreducible representations of the C_{2v} symmetry group).

TABLES

Configuration	Coefficient c_i
| 222220 222000⟩	0.8670236
| 222200 222200⟩	-0.3348786
| 222020 222020⟩	-0.1620731
| 222220 220002⟩	-0.0811422
| 22+22- 22-00+⟩	-0.0779391
| 22-22+ 22+00-⟩	-0.0779391
| 220222 222000⟩	-0.0731238
| 222000 222220⟩	0.0723549
| 222222 220000⟩	-0.0710389
| 22+22+ 22-00-⟩	0.0620807
| 22-22- 22+00+⟩	0.0620807
| 220220 222002⟩	-0.0566175

TABLE II: Singlet CASSCF wavefunction at the transition state geometry, $\Psi = \sum_i c_i \mid ...\rangle$. All coefficients c_i having a modulus greater than 0.05 are given. Second quantized notation in two irreps, see text. C_2 symmetry used.

FIGURE CAPTIONS

- Fig.1 Isosurface 0.10 of the EPLF for O_4 at the equilibrium geometry using a HF trial wave function.
- Fig.2 Isosurface 0.11 of the EPLF for O_4 at the equilibrium geometry using a truncated CASSCF(16,12) trial wave function.
- Fig.3
- Fig.4
- Fig.5
- Fig.6
- Fig.7 Isosurface 0.09 of the EPLF for the singlet O_3 fragment using a HF trial wavefunction.
- Fig.8 Isosurface 0.09 of the EPLF for the singlet O_3 fragment using a truncated CASSCF(16,12) trial wavefunction.
- Fig.9

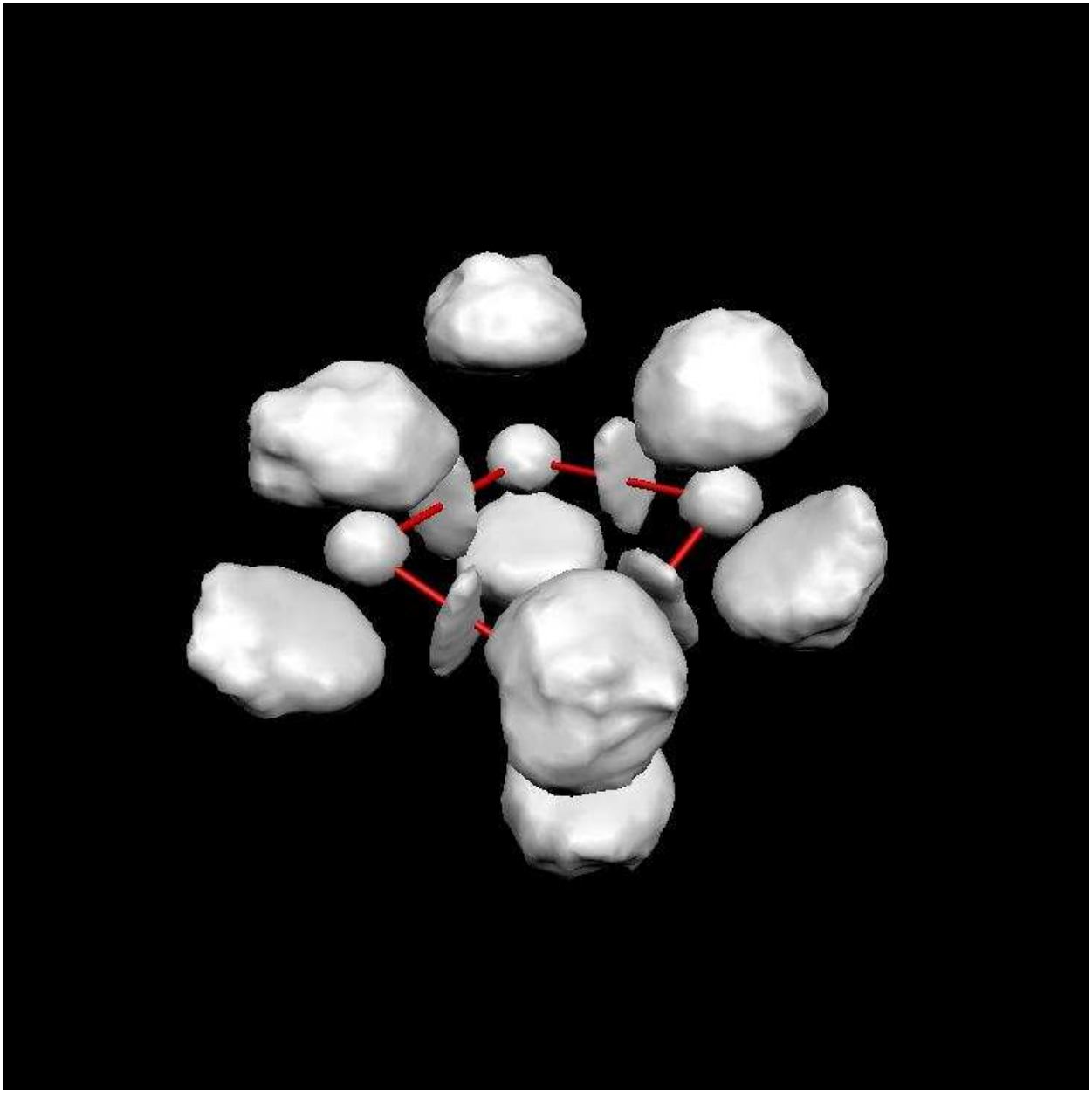

FIG. 1:

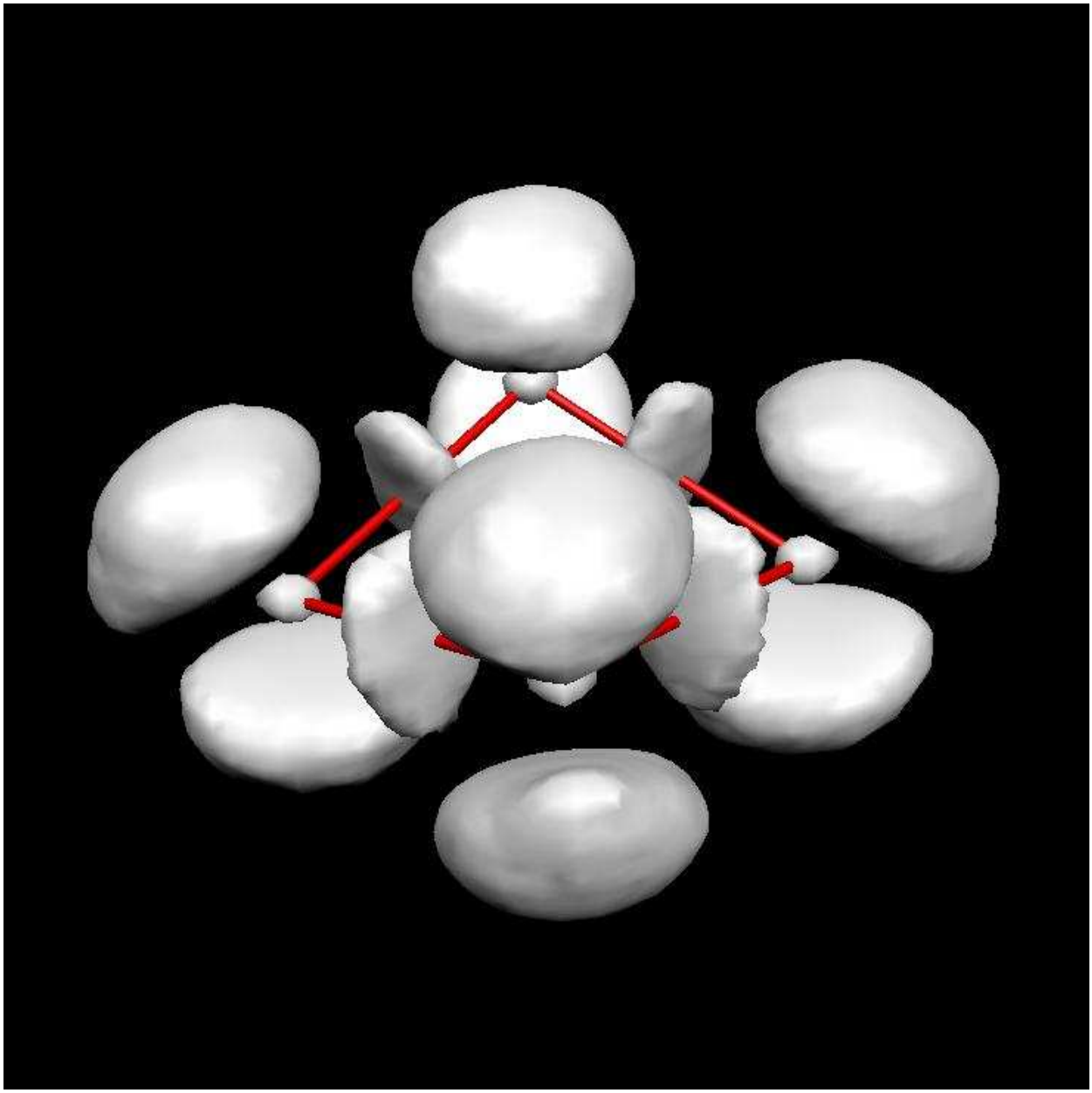

FIG. 2:

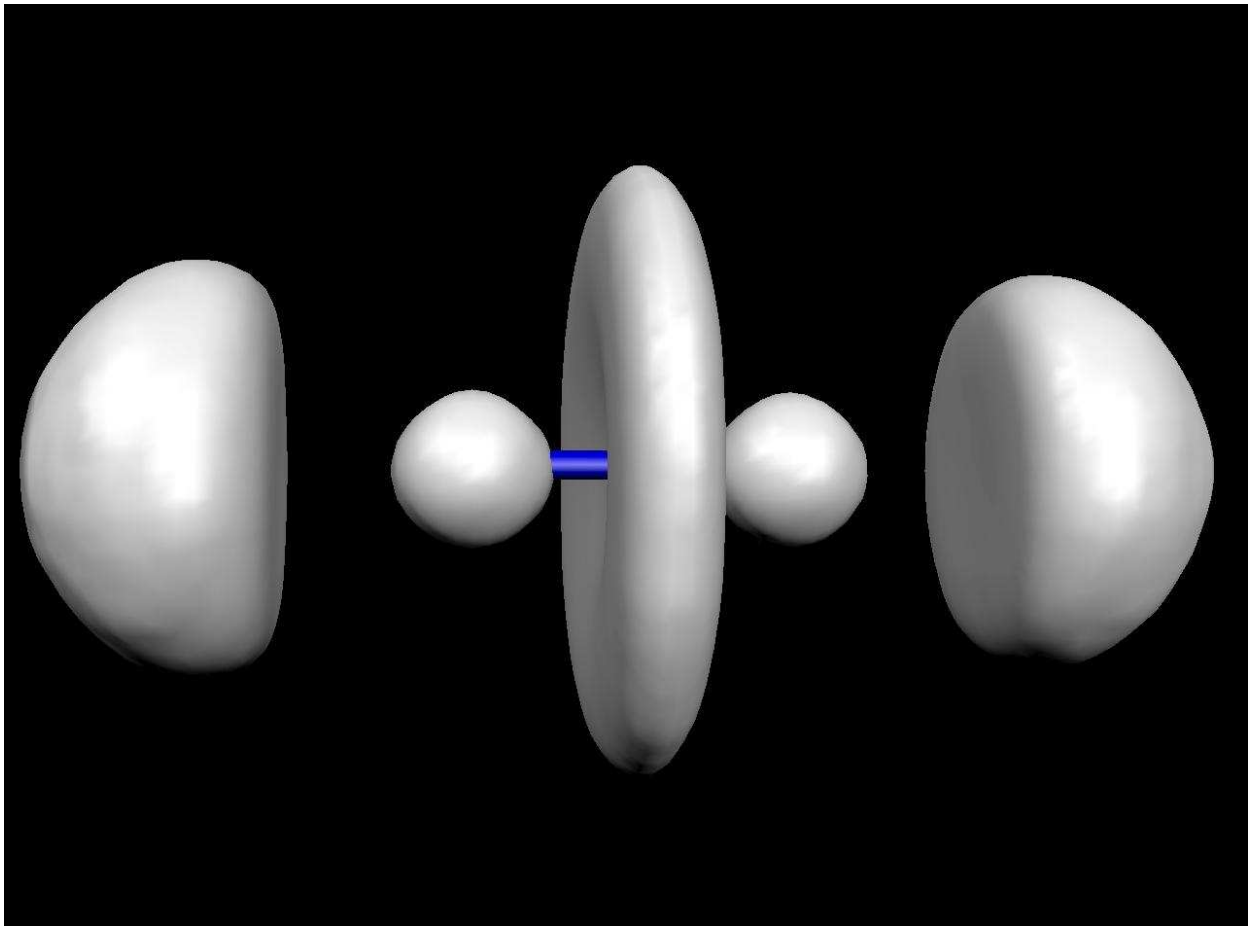

FIG. 3:

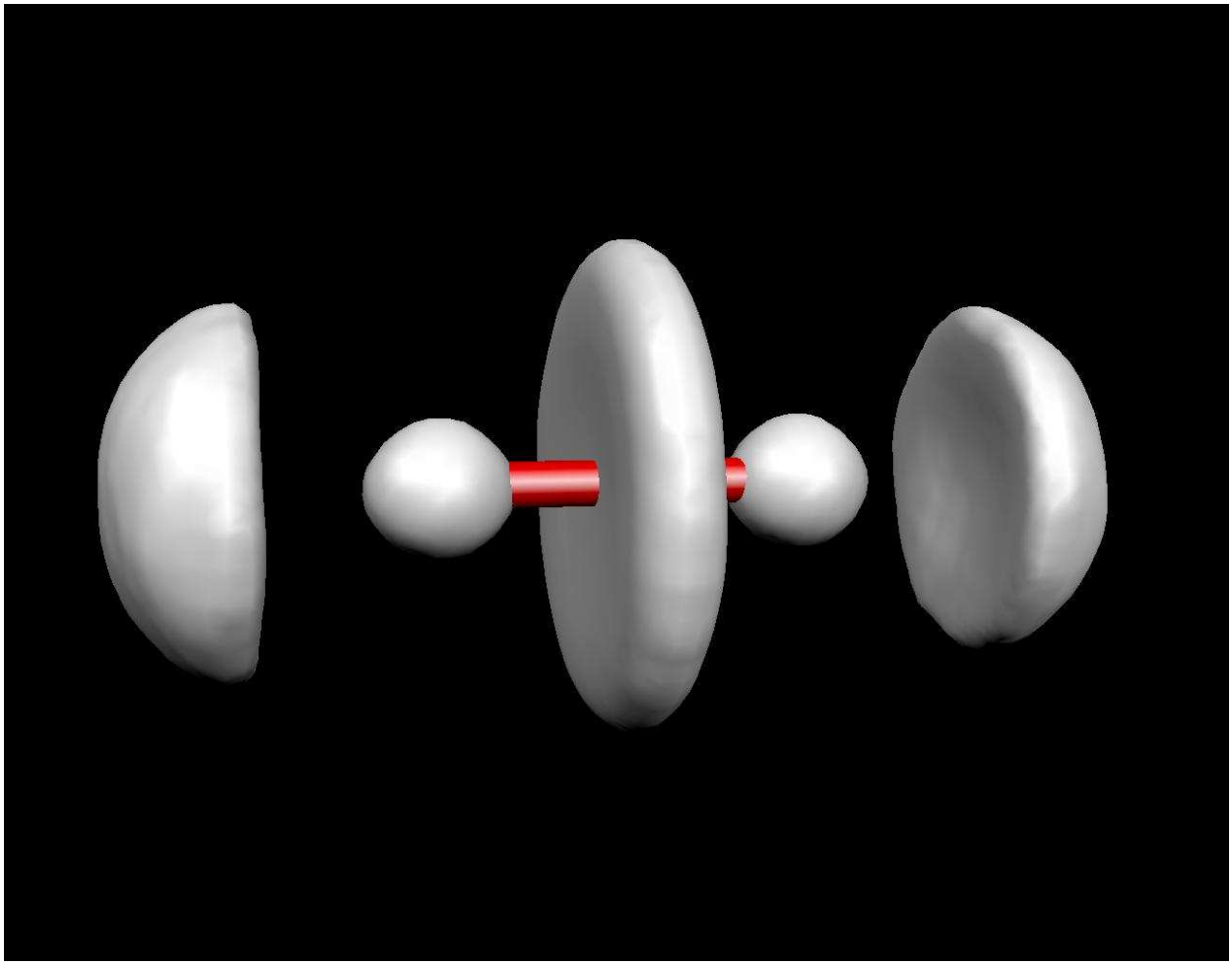

FIG. 4:

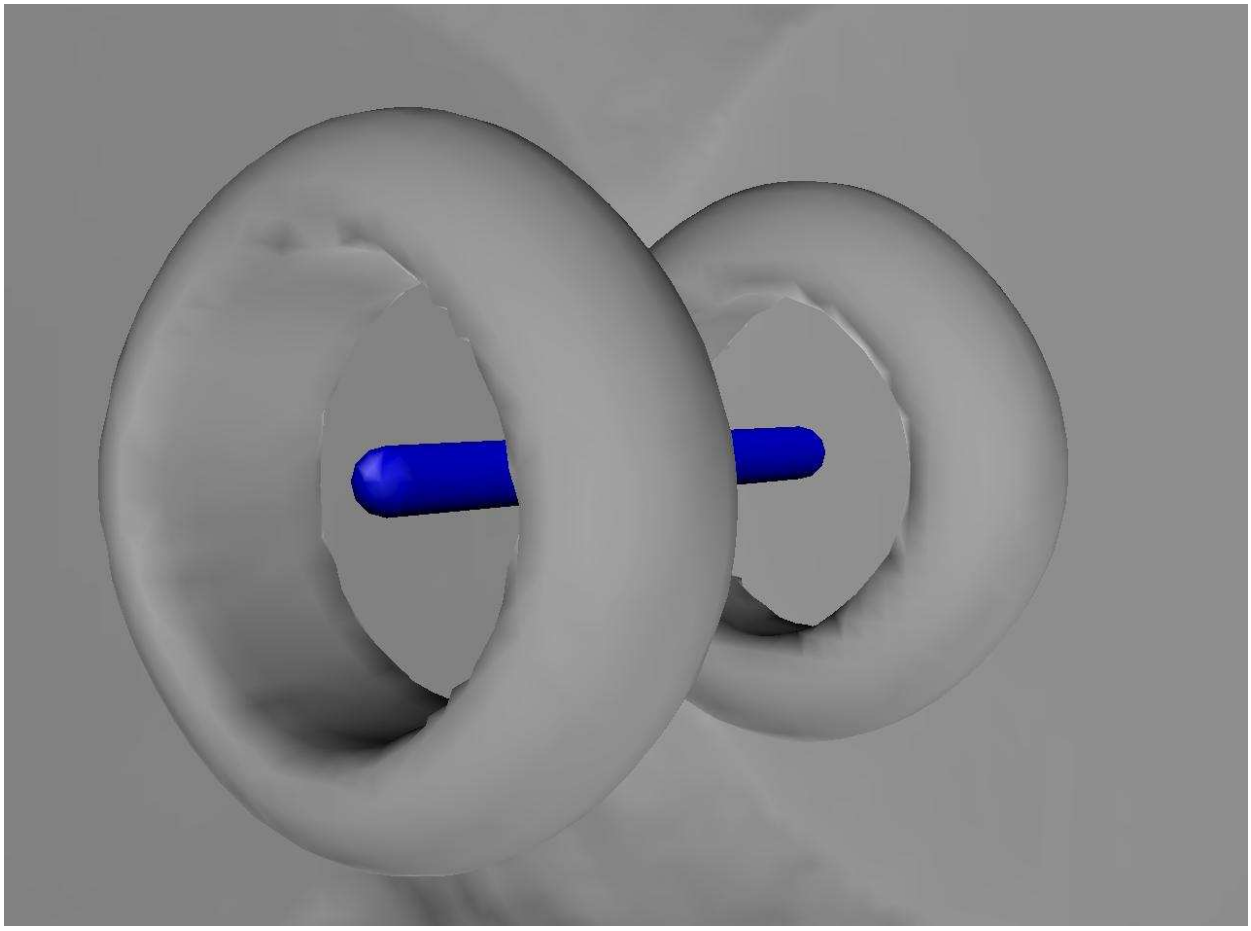

FIG. 5:

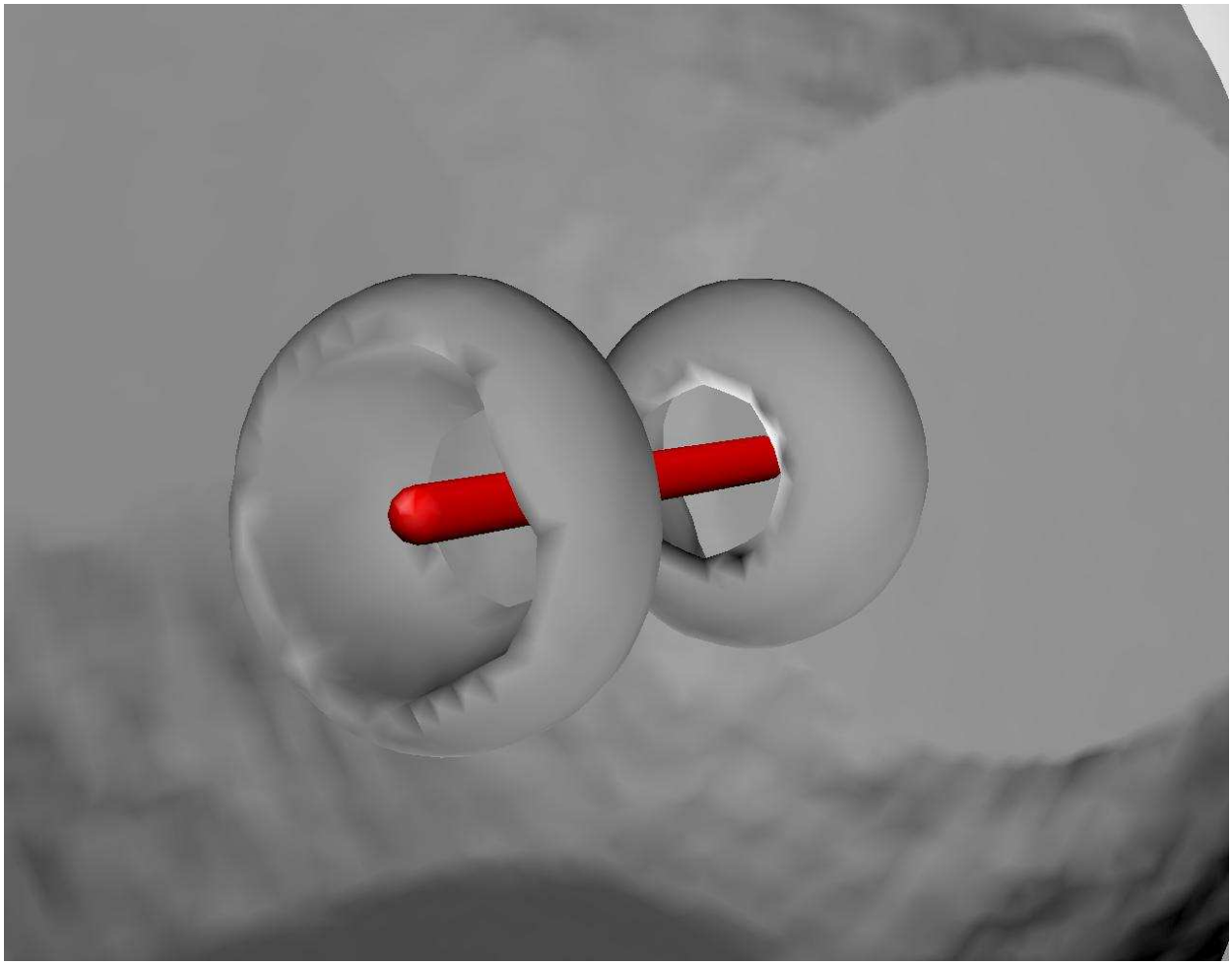

FIG. 6:

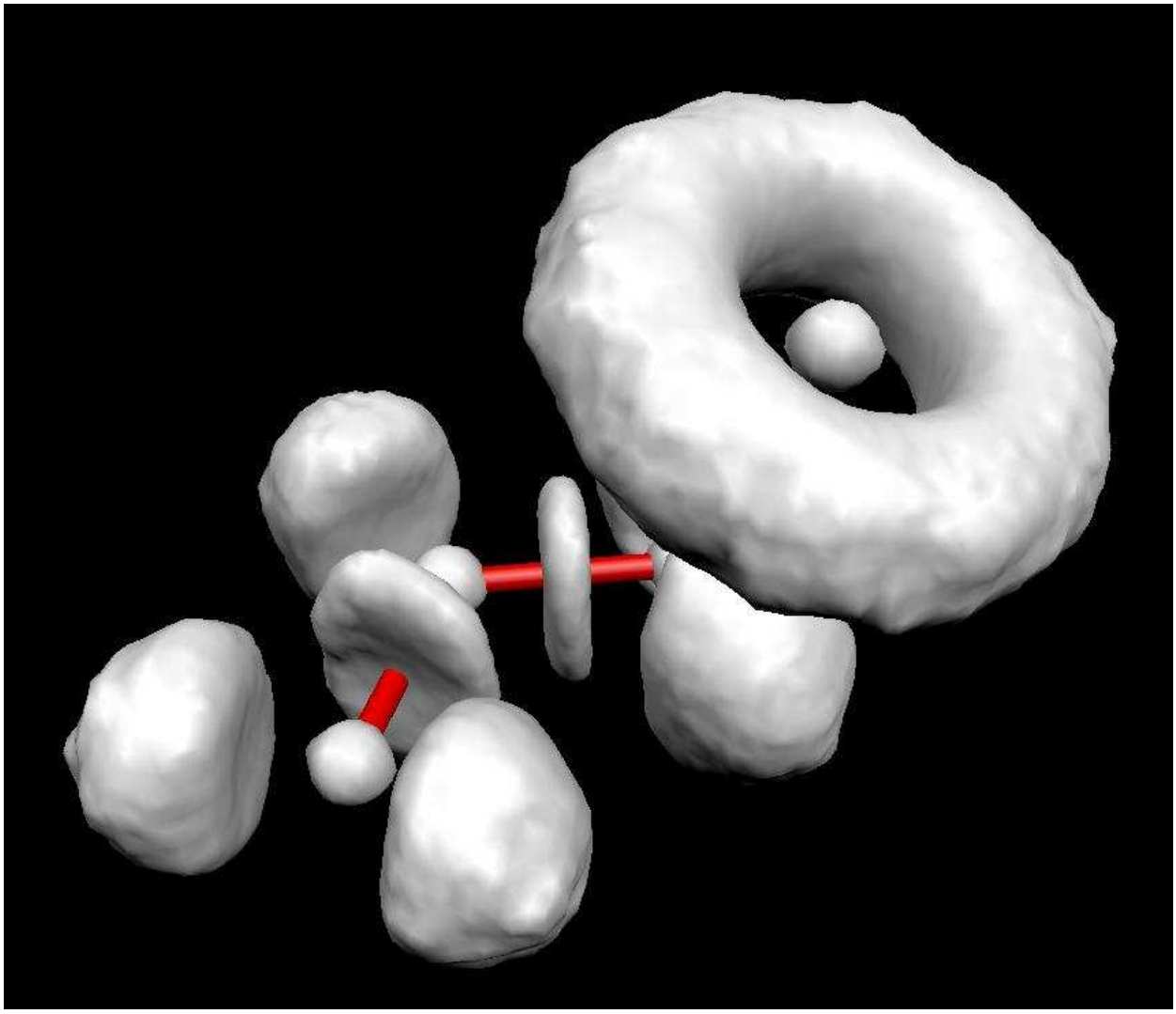

FIG. 7:

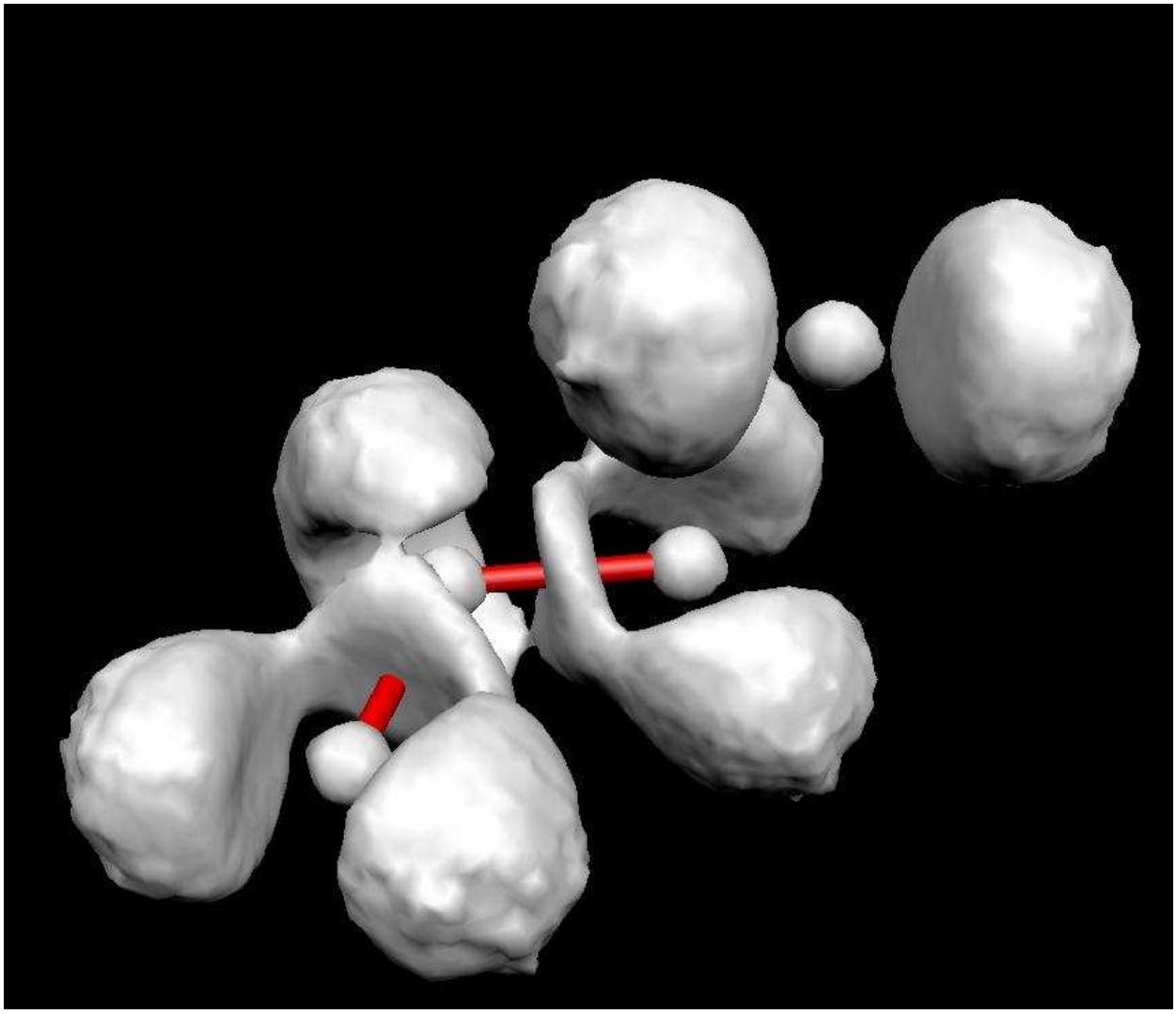

FIG. 8:

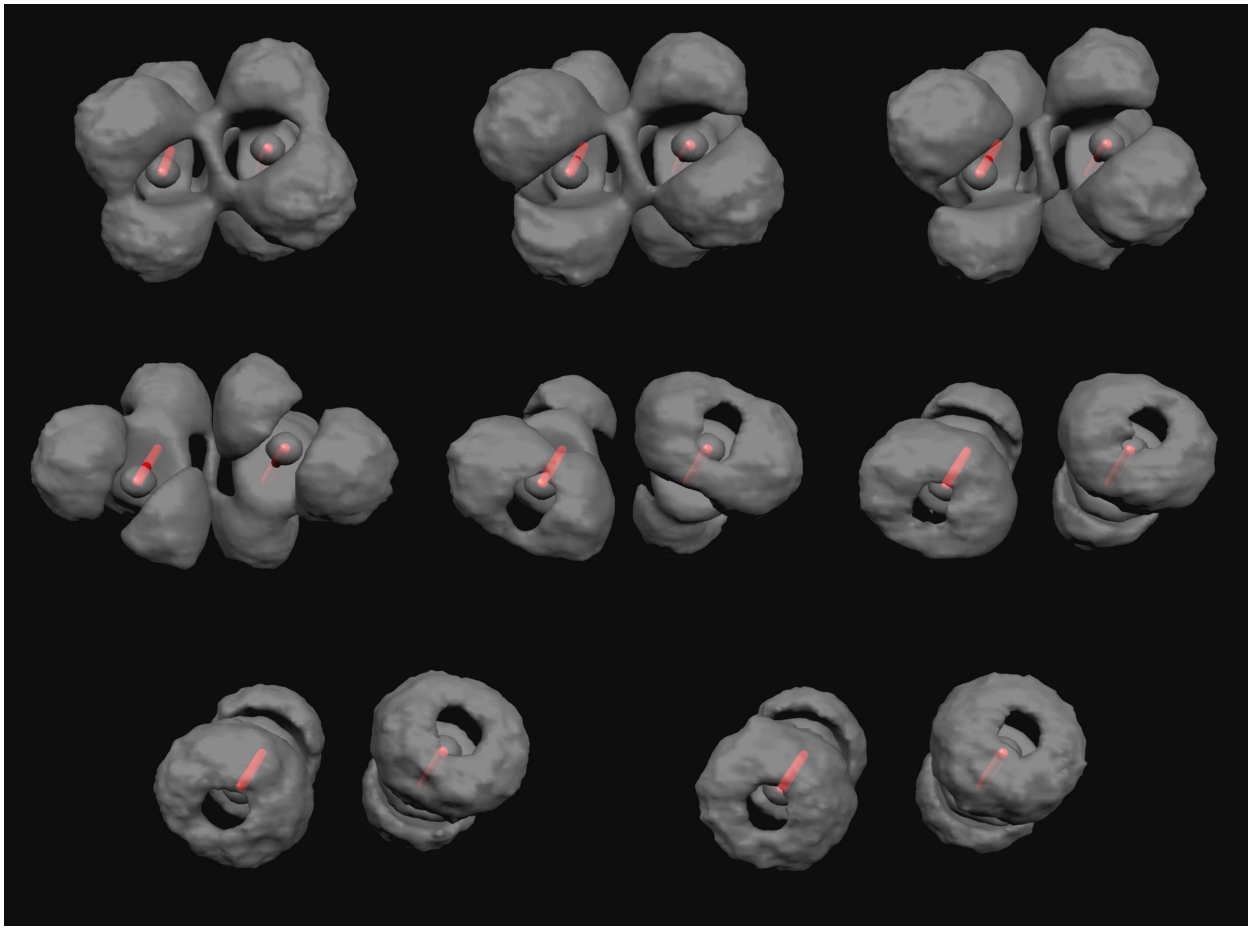

FIG. 9: